Multimode microscopy: spectral and lifetime imaging

Christian Blum, Yanina Cesa, Maryana Escalante and Vinod Subramaniam

J. R. Soc. Interface 2009 **6**, S35-S43
doi: 10.1098/rsif.2008.0356.focus

J. R. Soc. Interface (2009) 6, S35–S43
doi:10.1098/rsif.2008.0356.focus

Review

Multimode microscopy: spectral and lifetime imaging

Christian Blum*, Yanina Cesa, Maryana Escalante and Vinod Subramaniam*

Biophysical Engineering Group, Faculty of Science and Technology,
MESA+ Institute for Nanotechnology, University of Twente, P.O. Box 217,
7500 AE Enschede, The Netherlands

Multimode microscopy exploits the measurement of multiple spectroscopic parameters to yield a wealth of spatially resolved spectroscopic detail about the sample under study. Here, we describe the realization of a multimode microscope capable of wide-field transmission, reflectivity and emission imaging. The instrument also incorporates confocal spectral and lifetime imaging enabling convenient high-content imaging of complex samples, allowing the direct correlation of the data obtained from the different modes. We demonstrate the versatility of this imaging platform by reviewing applications to the modulation of fluorescent protein emission by inverse opal photonic crystals, to the detection and visualization of J-aggregate coupling of small molecule dyes intercalated into nanochannels in zeolites and to the visualization of fluorescent proteins micropatterned onto surfaces. In all cases, the combination of different microspectroscopic modes is essential for the resolution of specific photophysical details of the complex systems in question.

Keywords: spectral imaging; lifetime imaging; fluorescent proteins; micropatterning; zeolites; photonic crystals

1. INTRODUCTION

Advanced optical microscopy methods are routinely used for spatially resolved localization and visualization of optical contrast generating probes in various media. Nevertheless, these methods are of limited use in their ability to analyse the dynamics, interactions and physical environment of molecules when unassisted by spectroscopy. Imaging spectroscopy methods enable the extension of simple spatial analyses to demonstrate function, co-localization and molecular interaction. To this end, we are interested in combining different modes of microscopy with spectroscopic tools to better study molecular interactions. Our focus has been on exploiting the sensitivity and specificity of fluorescent probes to exploit the full repertoire of fluorescence phenomena (encompassing spectra, lifetimes, polarization and other parameters) in an imaging mode to yield spatially, spectrally and temporally resolved information about molecular systems of interest. Fluorophores may be used to probe proximity relationships through fluorescence resonance energy transfer, molecular interactions through polarization dynamics and characteristics of the molecular environment through fluorescent lifetime and emission spectra. Imaging spectroscopy can easily be extended to single-molecule imaging techniques and indeed provides essential information about spectral diffusion processes that occur in complex biomolecular systems.

Several laboratories have reported the design and implementation of integrated multi-parameter microscopy systems to simultaneously, or in a correlated manner, observe and image different emission parameters. Spectral and lifetime microscopy has been implemented in scanning microscopy using different detection techniques resulting in the acquisition of decay characteristics in certain wavelength windows and of emission spectra on a pixel or line basis (Bird *et al.* 2004; Qu *et al.* 2006; De Beule *et al.* 2007; Ruck *et al.* 2007). Wide-field detection schemes enabling spectrally resolved fluorescence lifetime microscopy have also been developed (Hanley *et al.* 2002; Nair *et al.* 2006). At the single-molecule level, multi-parameter detection strategies have been used to extract the full range of parameters (intensity, spectra, lifetime, polarization) characteristic of fluorescence emission to gain fundamental insights into the analysed systems (Kuhnemuth & Seidel 2001; Tinnefeld *et al.* 2001; Widengren *et al.* 2006).

These integrated multi-parameter imaging and spectroscopy developments have been applied to a

---

*Authors for correspondence (c.blum@tnw.utwente.nl, v.subramaniam@tnw.utwente.nl).

One contribution of 9 to a Theme Supplement 'Quantitative fluorescence microscopy: The 1st international Theodor Förster lecture series'.

Received 21 August 2008
Accepted 7 November 2008

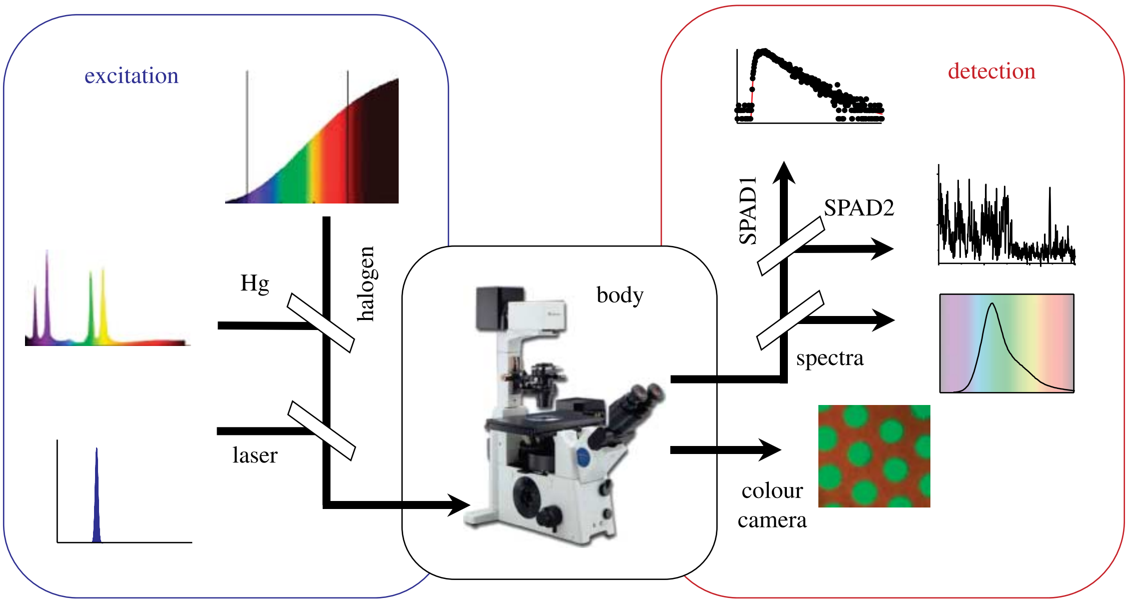

Figure 1. Schematic of the multimode microscope. The set-up is designed for maximum flexibility with different illumination (wide-field transmission or epi-illumination by halogen or mercury lamp, pulsed laser for confocal illumination) and detection (true colour intensity, spectra, lifetimes) possibilities. The sample is mounted on a scanning stage for raster scanning applications. Raster scanning the sample and spectral or lifetime determination per pixel yields spectral or lifetime images.

diverse set of problems, ranging from the analysis of dynamic processes in cells (Kudryavtsev *et al.* 2007; Ruck *et al.* 2007) to the analysis of dye coupling in inorganic scaffolds (Busby *et al.* 2008). In hybrid combinations with non-optical techniques such as scanning probe nanomanipulation, multi-parameter imaging has been used to study the structure, function and conformational changes of macromolecules (Kassies *et al.* 2005; Gaiduk *et al.* 2007).

Here, we review the design and application of a multimode microscope combining wide-field transmission, reflectivity and emission imaging with confocal spectral and lifetime imaging enabling convenient high-content imaging of complex samples, allowing the direct correlation of the data obtained from the different modes.

2. MULTIMODE MICROSCOPE: TECHNICAL DETAILS

We have realized a custom-built microscope incorporating spectroscopic capabilities for multimode fluorescence microscopy. The instrument combines wide-field emission imaging with scanning-stage confocal microscopy for fluorescence lifetime and spectral imaging.

The set-up is designed for maximum sensitivity resulting in single-molecule detection capability in the confocal branch of the microscope. The excitation laser, scanning stage and the different detectors of the confocal microscope are synchronized and controlled by a custom-built LabVIEW program. Key spectroscopic modes are spectral (Hiraoka *et al.* 2002; Zimmermann *et al.* 2003; Garini *et al.* 2006) and lifetime imaging (Suhling *et al.* 2005; Becker 2006), in which the sample is raster scanned and a full emission spectrum or decay curve, respectively, is recorded for each sampled point. The data acquisition overhead for a scanning technique generating vast numbers of spectra or decay curves, even when imaging small areas or at low lateral resolutions, renders this approach inherently slow. However, the achievement of single-molecule sensitivity in the instrument has a direct consequence for image acquisition times, and enables reasonably rapid acquisition of spectral and temporal information at high spatial resolution, even from samples containing relatively low concentrations of emitters.

A schematic of the multimode microscope is shown in figure 1, focusing on the three main modules of the set-up: excitation; microscope body; and detection.

The central part of the set-up is an inverted research microscope (Olympus IX71; Japan). The modular frame and optical design provide several access ports for multiple input or output devices convenient for multimode fluorescence microscopy.

The sample stage is a multi-axis, piezoelectric nanopositioning scanning stage (P-527.3CD; PI, Germany) of 200 μm lateral and 20 μm axial travel range, controlled by a digital controller (PI E710; PI, Germany). Integrated capacitive feedback sensors monitor the position of the stage and result in a scanning resolution of better than 2 nm and a full-range repeatability of 10 nm. The repeatability is particularly important for single-molecule detection applications, in which the emitters are first rapidly localized in a confocal scan and then revisited sequentially for further detailed analysis. The travel range of the stage is sufficiently large to accommodate larger structures such as crystals or cells, while the z-scanning capability allows for the acquisition of confocal slices.

Wide-field illumination can be achieved either by standard transmission illumination by a lamp mounted on the illumination column above the sample stage or in an epi-illumination configuration through the backport of the microscope. This combination enables work with transparent as well as non-transparent substrates or samples.

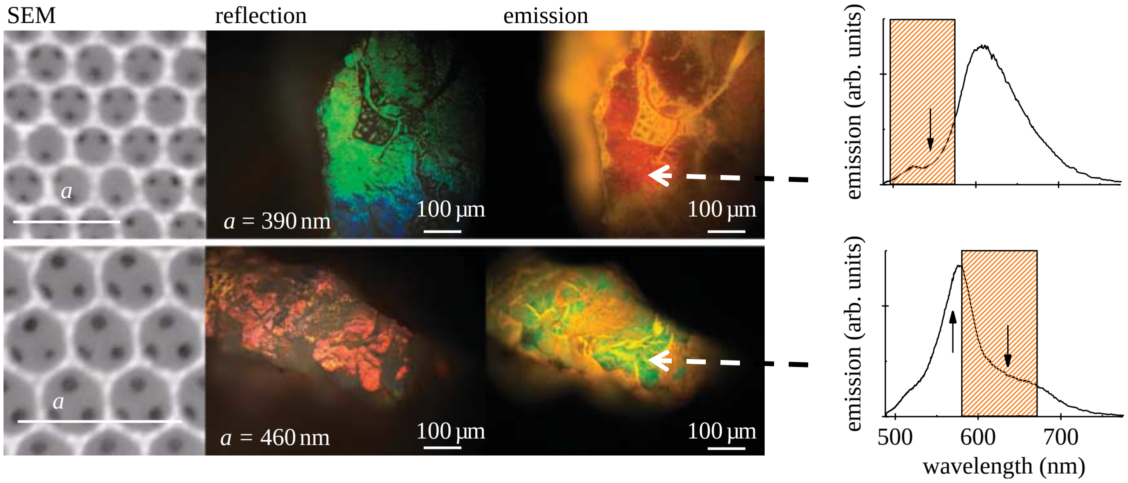

Figure 2. Control of the apparent emission colour of the fluorescent protein DsRed2 by photonic crystals. Typical SEM pictures from titania inverse opal photonic crystals (first column). The structure of air spheres (grey circles) supported by a backbone of titania (white) is clearly visible. The black spots are windows to the next layer of the crystal. The properties of the photonic crystal change with the air sphere size. The white light reflectivity pictures (second column) show the shift of Bragg-diffracted light from green to red with increasing lattice parameter. Synchronously, the apparent emission colour of fluorescent protein DsRed2 infiltrated into the crystals changes dramatically from red to bright green (third column). The emission colour of DsRed2 without photonic modification is orange/yellow as can be seen in some parts of both crystals where there is no photonic effect due to low crystal order. The emission spectra (fourth column) explain the observed effect. The wide stop-band modifies the directional emission spectrum. In the $a = 390$ nm crystal, attenuation in the green is observed at approximately 535 nm. This suppression of green components yields the red appearance of the protein emission. In the $a = 460$ nm crystal, the emission is strongly attenuated in the red at approximately 630 nm, and at the same time strongly enhanced at the short wavelength side of the spectrum. Both attenuation and enhancement together result in the observed change in emission colour.

Three different illumination sources can be conveniently selected by means of flip mirrors for wide-field and scanning microscopy (figure 1). A halogen lamp (Olympus, Japan) is used for wide-field reflectivity (epi-illumination) or transmission imaging. A mercury lamp (Olympus, Japan) is used for wide-field emission imaging. The fluorescence filter cubes of the microscope provide the necessary excitation and emission selectivities. For scanning applications, a variable repetition rate pulsed diode laser (BDL475, 469 nm; B&H, Germany) is used, and enables time-resolved fluorescence measurements using time-correlated single-photon counting (TCSPC). A set of attenuators in the excitation path allows incident power control, and an extra long pass filter (razor edge 473.0 nm, Semrock, USA) in the emission path suppresses any remaining reflected and scattered excitation light.

The flexibility in source selection (figure 2) was exploited for correlated reflection and emission imaging and spectroscopy of fluorescent proteins embedded in photonic crystals (Blum *et al.* 2008), and is reviewed in section 3.1.

The detection module is divided into wide-field and confocal detection branches. For wide-field imaging, we use a sensitive colour camera (AxioCam HRC; Zeiss, Germany), combining very low noise, maximum dynamic range and high sensitivity with high resolution and fast read-out. The high dynamic range and sensitivity make the camera suitable for both low light-level emission imaging and transmission and reflectivity imaging, which typically involve much higher light levels.

In the confocal configuration, rejection of out-of-focus light is obtained by using a pinhole aperture in a conjugate focal plane to the specimen and minimizing the excitation volume using diffraction-limited spots with high numerical aperture objectives. Full emission spectra or emission decay characteristics can be measured, and may be conveniently selected by means of flip mirrors. In principle, simultaneous spectral and lifetime imaging is also possible.

The emission spectra can be recorded by dispersing the emitted light via a prism-based custom-built spectrometer onto a spectroscopic camera. In this way, the full emission spectrum from the sampled spot can be recorded with high spectral resolution of approximately 1 nm in a single shot eliminating wavelength scanning and photon wastage. We chose for a prism-based spectrometer because of the somewhat higher transmission compared with grating-based spectrometers. The camera to record the emission spectra (Newton DU97N-BV; Andor, Northern Ireland) is optimized for spectral applications (chip size 1600 × 400 pixels) and delivers quantum efficiencies above 50 per cent between 400 and 900 nm with 95 per cent quantum efficiency at approximately 500 nm. Thermoelectric cooling up to −70°C results in negligible dark current. The camera can be used in a conventional mode by directly reading out the charges from each pixel or in an electron multiplying mode, in which the charge from each pixel is multiplied on the sensor before read-out for maximum signal-to-noise ratio. Wavelength calibration is achieved using a calibrated light source (Cal-2000 Mercury Argon Calibration source; Ocean Optics, USA). In principle, one emission spectrum can be read out every few milliseconds; however, typical times to record an emission spectrum range from some tens of milliseconds for strongly emitting samples to hundreds of milliseconds for a single-molecule emission spectrum.

The second detection possibility in the confocal branch of the microscope is the detection of emitted photons by single-photon avalanche diodes (SPAD). SPADs are spectrally integrating detectors that count the number of arriving photons irrespective of the wavelength of the photons. The chosen SPADs (PDM series, MPD, Italy) efficiently detect in the wavelength region between 400 and 750 nm with a peak quantum efficiency of approximately 50 per cent at 500 nm. The SPADs used also provide a better than 50 ps FWHM timing resolution that allows for the precise determination of the arrival time of single photons at the detector, which is necessary for the lifetime determination of emitters. In our set-up, we currently have two SPADs that can be separated, for example, by a polarizing beam splitter for polarization-sensitive measurements, by a dichroic mirror for dual-wavelength channel detection or by a beam splitter for photon anti-bunching experiments.

The two SPADs serve as inputs for a TCSPC module (SPC-830; Becker & Hickl, Germany) enabling time-resolved fluorescence measurements. TCSPC with pulsed lasers yielding short pulses provides fluorescence lifetime measurements with excellent time resolution, and can be used for ensemble as well as single-molecule samples. In ensemble samples, the TCSPC criterion of having utmost one photon arriving at the detector per excitation pulse is achieved by controlling the excitation intensity or detection efficiency, whereas single molecules inherently can only emit one photon per excitation cycle.

The SPC-830 module can be operated in several modes such as single/oscilloscope, scan and first-in first-out (FIFO). In the basic modes, the emission intensity decay is measured and recorded. A series of '$f(t,\text{parameter})$' modes give the possibility to follow decay curve changes over different parameters at a fixed point in the sample. Decay curve changes as a function of time or of external parameters such as wavelength or displacement can be followed for a single detector or an array of detectors. A series of 'scan' modes in combination with the scanning-stage system are used for image recording. In the FIFO mode, for each detected photon, the time within the laser pulse sequence, the time from the start of the experiment and the number of the detector channel that received the photon are recorded. These results can be used to calculate fluorescence correlation spectra, decay curves and photon counting histograms as a function of time, giving the possibility to study the dynamics of the fluorescence system, such as lifetime fluctuations, over a wide range of time scales. The lifetime data are analysed using the Becker & Hickl SPCImage software package (Becker 2006).

3. MULTIMODE MICROSCOPY: APPLICATIONS

As outlined above, we have incorporated a commercial inverted microscope into a versatile custom-built set-up enabling multimode microscopy including steady-state and time-resolved fluorescence measurements to yield correlated high-content spectroscopic imaging of complex samples. The versatility of this multimode imaging platform, and of multi-parameter imaging in general, is demonstrated in three applications at the interfaces of different disciplines.

3.1. Biophotonic engineering: nanophotonics to manipulate emission from proteins

We have used the multimode microscope described here to study, for the first time, the manipulation of biological emitters by the rapidly growing toolbox of nanophotonics, by investigating the control of the emission colour of fluorescent proteins by photonic crystals (Blum *et al.* 2008).

Photonic crystals are nanostructured periodic dielectric composites containing spacings comparable to the wavelength of light that control light propagation, in particular crystallographic directions by means of Bragg diffraction. This results in wavelength ranges—called stop-bands—for which light cannot propagate within the crystal, so that the incoming light in this wavelength range is reflected (Miguez *et al.* 1999). At the same time, stop-bands also modify the emission spectra of emitters embedded inside photonic crystals and give rise to directional enhancement or attenuation of emission (Nikolaev *et al.* 2005). The photonic crystals used were titania inverse opals, which consist of a three-dimensional structure of air spheres supported by a backbone of titania (for typical SEM images, see the first column of figure 2; Wijnhoven *et al.* 2001). The wavelength at which Bragg diffraction occurs is directly dependent on the lattice parameter a of the crystals, and hence the size of the air spheres. A number of different crystals with varying air sphere sizes and thus varying lattice parameter were prepared and analysed. White light was used to illuminate the crystals in a reflectivity configuration, and the light that was reflected from the crystal was imaged with a colour camera. The second column of figure 2 shows the change in reflected colour when the lattice parameter a is changed. Clearly, the wavelength at which Bragg diffraction occurs changes with increasing lattice parameter from green (a=390 nm) to red (a=460 nm) as the stop-band shifts from shorter to longer wavelength due to Bragg diffraction. Some areas of all the crystals do not efficiently reflect light, which is due to a lower crystal quality in these areas, preventing the formation of stop-bands (Wijnhoven *et al.* 2001).

In a second step, the emission from the red fluorescent protein DsRed2 infiltrated into the same photonic crystals was analysed by wide-field fluorescence microscopy. With increasing lattice parameter of the photonic crystals, the apparent emission colour changed dramatically from red to green as shown in the third column of figure 2. Correlating the white light reflection and the emission pictures showed that the change in emission colour only occurred in the areas in which colourful reflection due to Bragg diffraction was observed. The areas that stayed dark in the reflection image did not show any colour change in the emission picture, and in these areas the typical orange/yellow colour of the unmodified protein emission was observed.

To further illuminate the observed dramatic colour change in the apparent DsRed2 emission, local emission spectra from highly photonic areas of the sampled crystals are presented in the fourth column of figure 2. It is precisely the ability of multimodal imaging to provide complementary images and spectroscopic information in perfect register that leads to the explanation of the observed phenomenon. For the $a=390$ nm crystal, the reflectivity picture shows green reflection and consistently attenuation near 535 nm resulting from the broad photonic stop-band. Attenuation in the green wavelength area at approximately 535 nm in the DsRed2 emission changes the apparent emission colour from the typical orange/yellow of the unmodified emission to the strong red emission observed.

For the $a=460$ nm crystal, the stop-band has shifted to 630 nm, which is confirmed by the red reflection seen in the reflectivity picture. The spectrum shows that the emission spectrum is attenuated over a wide range in the red part of the emission, while the green part of the spectrum is decidedly enhanced. The combination of attenuating the red part of the spectrum while at the same time enhancing the green part of the emission spectrum results in the dramatic change in apparent emission colour to bright green (third column of figure 2).

The analysis of the emission spectra confirmed that the systematic shift of the photonic stop-band through the emission spectrum of the fluorescent protein DsRed2 explains the observed drastic colour changes. The changes in the emission spectra are strong, and attenuation of up to 80 per cent in the photonic stop-band as well as enhancement of up to 50 per cent on the blue side of the stop-band was observed, which is in excellent agreement with the theory (Koenderink & Vos 2003; Nikolaev *et al.* 2005). The observed enhancement is due to Bragg diffraction at higher angles resulting in the escape of shorter wavelength light in the direction of the detector. The simultaneous observation of attenuation and enhancement shows that the effect is not a simple filter action. The correlated appearance of both attenuation and enhancement within the same spectrum acts as photonic contrast enhancement, and is the basis of the observed remarkably strong changes in emission colour.

This work has shown the potential of using the toolbox of nanophotonics to manipulate the photophysics of biological systems. An important future perspective would be the tuning of energy trapping in photosynthesis through the manipulation of the competition between spontaneous emission and Förster energy transfer by photonic structures. Such an application would require correlated measurements of the fluorescence decay characteristics and emission spectra.

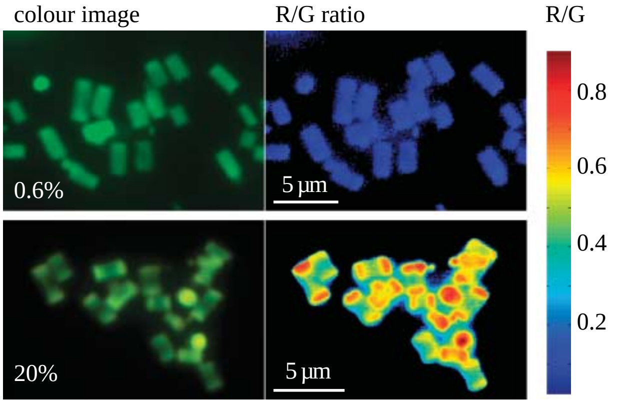

Figure 3. Wide-field imaging of pyronine intercalated zeolite L. The true colour images (first column) of 0.6% and 20% loaded zeolites (top and bottom row) show green emission from the intercalated pyronine, while the higher loaded crystals appear slightly more yellow. False colour imaging of the red colour channel divided by the green channel (second column) shows that the 0.6% loaded crystals have only minor red spectral contributions, and that there is no change in the red to green ratio across the crystals. However, the 20% loaded zeolites generally show higher red contributions, exhibiting a gradient decreasing from the ends to the centre of the crystals.

3.2. Guest–host systems: fluorescent dye organized in zeolites

We have used multimode imaging to demonstrate J-aggregate coupling between pyronine dye molecules inside the sub-nanometre one-dimensional nanochannels of zeolite L (Busby *et al.* 2008). Organizing molecules in a defined manner holds great promise to realize highly structured systems that exploit properties that only arise due to the defined molecular geometry. Zeolites have been used in various applications in photonics and optoelectronics (Vietze *et al.* 1998; Calzaferri *et al.* 2003; Alvaro *et al.* 2007). Zeolite L has a crystalline structure with internal sub-nanometre channels running through the crystal. Zeolite L assemblies are suitable hosts for fluorescent dyes (Megelski *et al.* 2001; Maas *et al.* 2003; Huber *et al.* 2007). The fluorescent dye pyronine has been shown to intercalate into zeolite L crystals in a way that the individual dye molecules are aligned at defined angles within the crystal channels (Megelski *et al.* 2001). Steric hindrance in the channels means that the pyronine molecules cannot slide over, or stack on top of each other, thus preventing excimer (Ramamurthy *et al.* 1993) and H-aggregate (Calzaferri *et al.* 2003) formation. However, an ‘end-to-end’ alignment of the guest molecules can be envisaged, which could result in J-aggregate-type coupling. Bulk fluorescence lifetime studies of pyronine-intercalated zeolite L have shown loading-dependent multi-exponential decays (Yatskou *et al.* 2003), indicating that the molecules may interact with each other or the environment.

To elucidate possible dye interactions within zeolite nanochannels, we performed correlated fluorescence microscopy, fluorescence lifetime and spectral imaging of single crystals. Two different samples of zeolite L with intercalated pyronine at concentrations of 0.6 and 20 per cent were analysed. Conventional wide-field epifluorescence microscopy with true colour imaging was the starting point to analyse the emission characteristics observed in bulk measurements. All crystals showed green emission from the intercalated pyronine as shown in the first column of figure 3. The 0.6 per cent loaded crystals were homogeneously filled, whereas the 20 per cent loaded crystals showed stronger emission at the ends of the crystals than in the middle of the crystals. Also, these crystals showed a barely

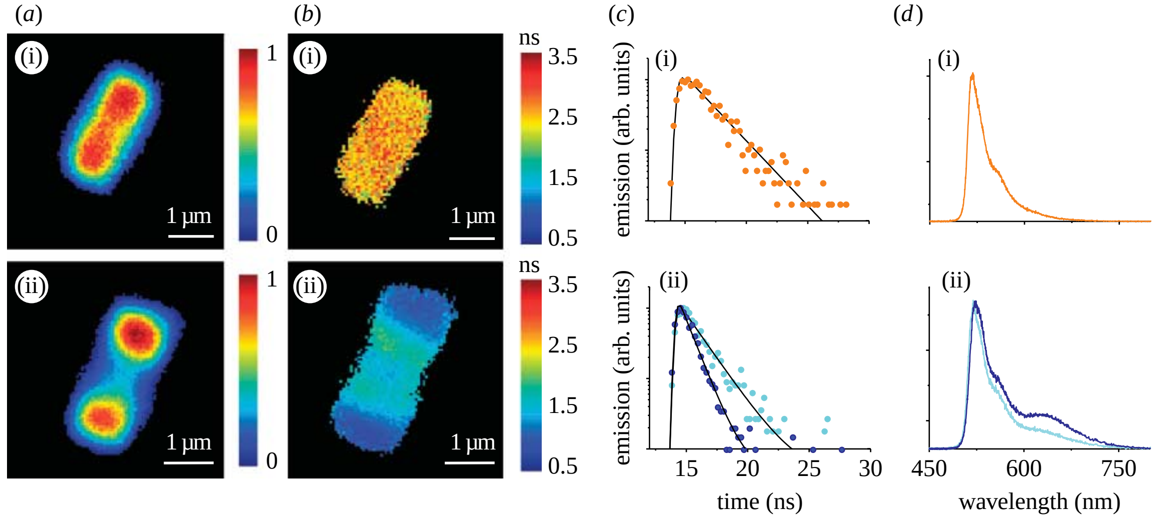

Figure 4. Lifetime and spectral imaging were performed on single pyronine intercalated crystals. Crystals with low pyronine loading of 0.6% (i) showed uniform emission intensity (*a*(i)), fluorescence lifetime (*b*(i)) and emission spectra (*d*(i)). Examples for decay characteristics (orange circles, =2.4 ns, (*d*(i))) and emission spectra are given in (*c*(i)) and (*d*(i)). Crystals with high pyronine loading of 20% (ii) show very different characteristics. A gradual decrease in emission intensity, (*a*(ii)), a gradual rise of emission lifetime (*b*(ii)) and a decreasing spectral band at approximately 650 nm (*d*(ii)) can be observed from the crystal ends to the centre. Typical decay characteristics ((dark blue circles, =1,0 ns and turquoise circles, =1.7 ns, (*c*(ii))) and emission spectra from the crystal ends (dark blue) and centre (turquoise) are given in (*c*(ii)) and (*d*(ii)). The observed changes are due to the formation of J-aggregates, with coupling predominantly occurring at the crystal ends where the local pyronine concentrations and thus the chances of dye interactions are larger than in the crystal centres.

noticeable yellow tinge, particularly at the ends of the crystals. By splitting the RGB channels of the camera output files and computing the ratio of the high (R channel) and low wavelength emissions (G channel), these colour variations were clearly highlighted for the 20 per cent samples, whereas the 0.6 per cent samples show no colour variation across the individual crystals (second column of figure 3).

Single crystals of samples with high and low pyronine loading were analysed using spectral and fluorescence lifetime imaging. For this purpose, the pulsed laser excitation was used and each crystal was imaged twice, once recording the decay curves and once recording the emission spectra, from each sampled point of the crystal. Figure 4 summarizes the results obtained.

The homogeneous filling of the 0.6 per cent crystals was confirmed by the intensity and fluorescence lifetime measurements. The emission spectra also showed no variation across the crystals. The measured decay characteristics fitted well to a monoexponential decay function with a lifetime distributed at approximately 2.6 ns, and no systematic variations in the fluorescence lifetime across the crystals could be observed (figure 4*a*(i),*b*(i)).

For the 20 per cent pyronine-loaded zeolite sample, a decidedly different picture was found as shown in figure 4*a*(ii),*b*(ii),*c*(ii),*d*(ii). Not only the emission intensity, but also the emission spectrum and the emission lifetime were clearly different between the crystal ends and the centres of each crystal. The intensity map shows a gradual decrease in intensity from its maximum at the plane of the channel entrances towards the middle of the crystal. This is attributed to a non-uniform doping of the crystals with very high dye concentrations at the channel entrances at the ends of the crystal and decreasing dye concentrations towards the channel centres. The spectral imaging of the crystals showed a direct correspondence between the shape of the emission spectra and the intensity gradient. At the highly concentrated ends of the crystals, a new emission band at 630 nm is distinctly visible, and was not observed for the crystals with low pyronine doping. The intensity of this red band decreased in sync with the overall emission intensity towards the centre of the crystals.

Fluorescence lifetime imaging showed that the emission decays are shorter (approx. 1 ns) at the crystal ends, while towards the centre a clear increase is seen up to 2 ns (figure 4*b*(ii),*c*(ii)). Between these two extremes, the lifetime follows an inverse relationship to the intensity.

These data were consistent with the formation of J-aggregates of the pyronine dyes. J-aggregate coupling results in red-shifted absorption and emission compared with the monomer and faster fluorescence lifetimes (Kobayashi 1996), characteristics that were reflected in the spectral and the lifetime measurements. The possibility to correlate this spectroscopic information with the intensity map on the crystal provided the link between the probability of aggregate formation and the local concentration of dye inside the channel. Furthermore, the new luminescence band with fast decay constant was seen at the ends of the crystals in the regions of highest loading, where the probability of achieving a dense packing is the highest. Clearly, most J-aggregate coupling is found towards the ends of the channels with decreasing chance of molecular interaction towards the centre of the crystals (figure 4).

The ability to use nanochannels to organize molecules in end-to-end excitonic arrangements provides new possibilities for both molecular and material designs. Furthermore, J-aggregate-type

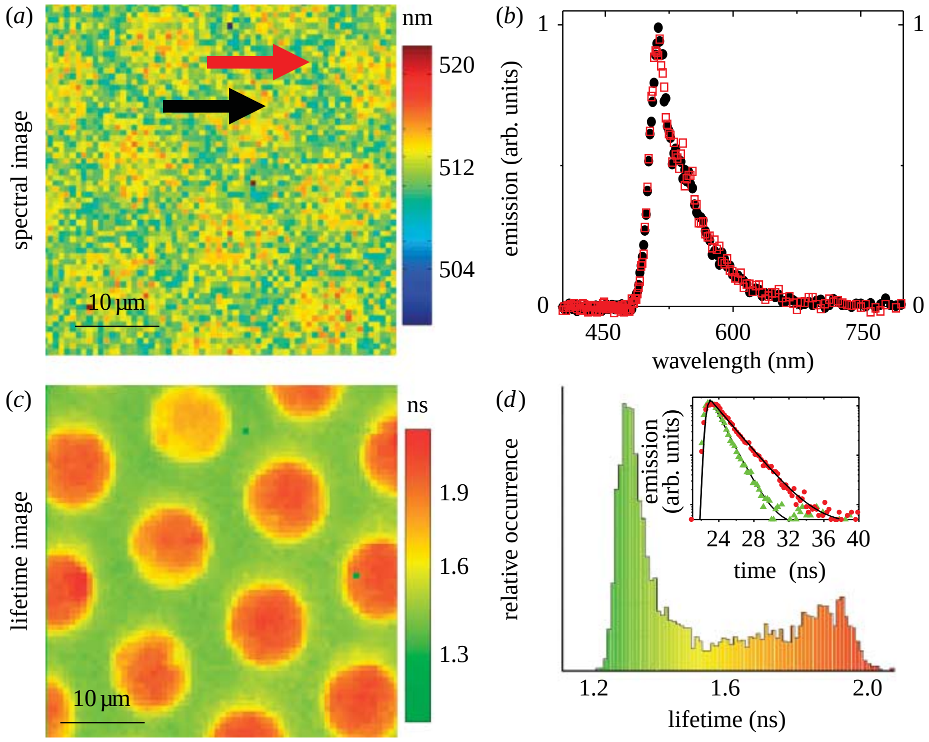

Figure 5. Two different fluorescent proteins patterned on a surface. The fluorescent protein EGFP was patterned onto a Ni:NTA glass-modified surface and then backfilled with the fluorescent protein RSGFP. (*a*) Spectral imaging of the sample (emission maximum position image) gives very low contrast, (*b*) since the two proteins show almost identical emission spectra. (*c*) The lifetime image confirms the successful patterning and functionality of the two proteins. (*d*) The lifetime histogram and typical decay curves. Inset: triangles, backfilled; circles, dot pattern.

interactions have implications on the dynamics of energy transfer and migration in mixed donor–acceptor zeolites used as artificial antenna systems (Calzaferri *et al.* 2003).

3.3. Protein patterning on surfaces: discrimination and control of functionality of different proteins

Ordered arrays of biomolecules on surfaces are of increasing interest for fundamental studies and applications in genomics and proteomics (Zhang *et al.* 2005). While DNA array technology is fairly well developed (Brockman *et al.* 1999), protein arrays often suffer from a loss of biological functionality due to the very process of surface immobilization. It is thus essential to validate the functional biological activity of surface immobilized proteins. The members of the class of visible fluorescent proteins (VFPs), such as the *Aequoria* green fluorescent protein (GFP) and its variants, are convenient test molecules to assess the success of various chemical patterning strategies. The fluorescence of VFPs is tightly coupled to their structural integrity, and the appropriate fluorescence signatures (spectra, lifetimes) are indicative of a functional protein (Ward & Bokman 1982). We have exploited optical microscopy and spectral imaging to validate the functional status of various proteins exhibiting fluorescence signatures patterned on the surfaces using different fabrication strategies, including microcontact printing and nanoimprint lithography, exploiting both non-specific and specific immobilization strategies (Maury *et al.* 2007; Ludden *et al.* 2008; Escalante *et al.* 2008*a*,*b*).

To highlight the power of multimodal imaging spectroscopy as realized in the system described in this paper, we demonstrate here the fabrication and characterization of a mixed array of two spectrally identical VFP variants, but which demonstrate clear differences in fluorescence lifetime. We show that the fluorescence lifetime imaging delivers clear contrast between the two proteins, enabling their discrimination, an exercise otherwise impossible by conventional imaging or spectral imaging methods.

We have used two variants of the *Aequoria* GFP, the enhanced GFP (EGFP) and a spectrally almost identical protein termed RSGFP. Both variants possess an engineered 6His affinity tag enabling specific immobilization onto glass substrates modified with Ni:NTA chemistry. The substrates were microcontact printed with EGFP, followed by stamp removal and backfilling of the substrates with an RSGFP solution, yielding a mixed array of specifically bound EGFP and RSGFP.

Epifluorescence microscopy of the patterned substrate yields a characteristic green fluorescence image across the whole surface. A spectral image of the patterned proteins, depicting the emission peak positions of the spectra, as shown in figure 5*a*, shows little or no contrast, as expected. Normalized single-point emission spectra acquired at positions where either EGFP or RSGFP were immobilized are shown in figure 5*b*. The spectra are consistent with the characteristic emission spectra of these VFPs in solution, clearly demonstrating the structural integrity of the immobilized proteins, and are superimposable, thus highlighting the inability to discriminate the two different fluorescent proteins on the basis of the emission spectra.

A fluorescence lifetime image of the micropatterned protein array was performed, and the lifetime image presented in figure 5*c* was obtained by monoexponential fitting of the decay curves (SPCImage software). The fluorescence lifetime image clearly reproduces distinctive areas with different lifetime distributions, corresponding to a peak at approximately 2 ns for the dot pattern where the EGFP was immobilized by microcontact printing, and to a second peak at approximately 1.3 ns for areas backfilled with RSGFP. Characteristic decay curves from each distribution peak are shown in the inset of figure 5*d* with the respective monoexponential fitting curves. The monoexponential behaviour of the decay curves present in both areas of the pattern indicates no significant superposition of the two different proteins, and is an indicator of the quality of the selective immobilization on the surface.

The lifetime of approximately 1.3 ns measured for RSGFP was consistent with the value we measured for the same protein in solution. We note that this value is somewhat higher than that reported in the literature (Volkmer *et al.* 2000), and may reflect specific sample storage conditions and age. The values measured for EGFP are consistent with the literature and with those expected in the presence of a higher refractive index substrate.

The fluorescence lifetime image provides excellent contrast and enables the localization of the respective proteins to the expected regions of the pattern. Both spectral and lifetime imaging confirm the structural integrity of the proteins upon immobilization, while the latter mode yields spectroscopic contrast that is not achievable with fluorescence intensity or spectra.

These integrated microspectroscopic approaches could potentially be used to sensitively detect and characterize the binding of ligands or other proteins onto fabricated protein arrays. Possible applications could be to measure receptor–ligand interactions, antibody–antigen interactions or for the fundamental studies of proteasome activity on fluorescently labelled protein substrates using immobilized proteasomal components (Nikles & Tampe 2007; Turchanin *et al.* 2008).

4. SUMMARY

Although multimode microscopy holds great promise in the analysis of complex emitting systems, it remains an underused technique. We have reviewed in this contribution the concept and realization of a custom-built high-sensitivity multimode microscope capable of different wide-field and confocal imaging and spectroscopy modes. In the wide-field mode reflectivity, transmission and emission imaging are possible and can be correlated with high-resolution spectral and lifetime imaging in the confocal mode. The correlation of spectral, lifetime and intensity images is often crucial in the analysis of complex systems.

We have also reviewed three different applications on the interfaces of physical chemistry, biophysics, materials science and nanotechnology, highlighting the enormous promise of a microscope designed for maximum flexibility, highest sensitivity and multimode detection in elucidating the photophysical details of organic and biological emitting molecules in confined spaces on the nanometre scale and on surfaces. By incorporating spectroscopic modes into the microscope, we are able to gain insights into molecular interactions and their interactions with the surrounding host material and nanostructures. We believe that this combination of multimode imaging and spectroscopy has significant potential to be a new tool for deeper understanding of materials and interactions at the interface of different fields.

We thank Aufried Lenferink for the work on the design of the multimode microscope and for programming the control software. We acknowledge fruitful cooperation with Prof. Dr W. L. Vos on the photonic crystal work, with Profs. Luisa de Cola and Gion Calzaferri on the zeolite work and with Prof. Dr J. Huskens on the patterning of fluorescent proteins. We thank 'Stichting voor Fundamenteel Onderzoek der Materie' (FOM), which is supported by the 'Nederlandse Organisatie voor Wetenschappelijk Onderzoek' (NWO) and the Nanotechnology Network in The Netherlands (NANONED), for financial support. For the zeolite work, the collaboration between Westfälische Wilhelms-Universität Münster and the MESA+ Institute for Nanotechnology was supported by the FP6 Network of Excellence Frontiers under the contract no. NMP4-CT-2004-500328 FRONTIERS NoE.

REFERENCES

Alvaro, M., Cabeza, J. F., Corma, A., Garcia, H. & Peris, E. 2007 Electrochemiluminescence of zeolite-encapsulated poly(*p*-phenylenevinylene). *J. Am. Chem. Soc.* **129**, 8074–8075. (doi:10.1021/ja0718265)

Becker, W. 2006 *The bh TCSPC handbook*. Berlin, Germany: Becker & Hickl GmbH.

Bird, D. K., Eliceiri, K. W., Fan, C. H. & White, J. G. 2004 Simultaneous two-photon spectral and lifetime fluorescence microscopy. *Appl. Optics* **43**, 5173–5182. (doi:10.1364/AO.43.005173)

Blum, C., Mosk, A. P., Nikolaev, I. S., Subramaniam, V. & Vos, W. L. 2008 Color control of natural fluorescent proteins by photonic crystals. *Small* **4**, 492–496. (doi:10.1002/smll.200701160)

Brockman, J. M., Frutos, A. G. & Corn, R. M. 1999 A multistep chemical modification procedure to create DNA arrays on gold surfaces for the study of protein-DNA interactions with surface plasmon resonance imaging. *J. Am. Chem. Soc.* **121**, 8044–8051. (doi:10.1021/ja991608e)

Busby, M., Blum, C., Tibben, M., Fibikar, S., Calzaferri, G., Subramaniam, V. & De Cola, L. 2008 Time, space and spectrally resolved studies on J-aggregate interactions in zeolite-L nanochannels. *J. Am. Chem. Soc.* **130**, 10 970–10 976. (doi:10.1021/ja801178p)

Calzaferri, G., Huber, S., Maas, H. & Minkowski, C. 2003 Host-guest antenna materials. *Angew. Chem.-Int. Edit.* **42**, 3732–3758. (doi:10.1002/anie.200300570)

De Beule, P. *et al.* 2007 Rapid hyperspectral fluorescence lifetime imaging. *Microsc. Res. Tech.* **70**, 481–484. (doi:10.1002/jemt.20434)

Escalante, M. *et al.* 2008*a* Directed assembly of functional light harvesting antenna complexes onto chemically patterned surfaces. *Nanotechnology* **19**, 025 101. (doi:10.1088/0957-4484/19/02/025101)

Escalante, M. *et al.* 2008*b* Nanometer arrays of functional light harvesting antenna complexes by nanoimprint lithography and host–guest interactions. *J. Am. Chem. Soc.* **130**, 8892–8893. (doi:10.1021/ja802843m)

Gaiduk, A., Kuhnemuth, R., Felekyan, S., Antonik, M., Becker, W., Kudryavtsev, V., Sandhagen, C. & Seidel, C. A. M. 2007 Fluorescence detection with high time resolution: from optical microscopy to simultaneous force and fluorescence spectroscopy. *Microsc. Res. Tech.* **70**, 433–441. (doi:10.1002/jemt.20430)

Garini, Y., Young, I. T. & Mcnamara, G. 2006 Spectral imaging: principles and applications. *Cytometry A* **69A**, 735–747. (doi:10.1002/cyto.a.20311)

Hanley, Q. S., Arndt-Jovin, D. J. & Jovin, T. M. 2002 Spectrally resolved fluorescence lifetime imaging microscopy. *Appl. Spectrosc.* **56**, 155–166. (doi:10.1366/0003702021954610)

Hiraoka, Y., Shimi, T. & Haraguchi, T. 2002 Multispectral imaging fluorescence microscopy for living cells. *Cell Struct. Funct.* **27**, 367–374. (doi:10.1247/csf.27.367)

Huber, S., Ruiz, A. Z., Li, H. R., Patrinoiu, G., Botta, C. & Calzaferri, G. 2007 Optical spectroscopy of inorganic–organic host–guest nanocrystals organized as oriented monolayers. *Inorg. Chim. Acta* **360**, 869–875. (doi:10.1016/j.ica.2006.06.008)

Kassies, R., Van Der Werf, K. O., Lenferink, A., Hunter, C. N., Olsen, J. D., Subramaniam, V. & Otto, C. 2005 Combined AFM and confocal fluorescence microscope for applications in bio-nanotechnology. *J. Microsc.-Oxf.* **217**, 109–116. (doi:10.1111/j.0022-2720.2005.01428.x)

Kobayashi, T. 1996 *J-aggregates*. Singapore: World Scientific Publishing.

Koenderink, A. F. & Vos, W. L. 2003 Light exiting from real photonic band gap crystals is diffuse and strongly directional. *Phys. Rev. Lett.* **91**, 213 902. (doi:10.1103/PhysRevLett.91.213902)

Kudryavtsev, V., Felekyan, S., Wozniak, A. K., Konig, M., Sandhagen, C., Kuhnemuth, R., Seidel, C. A. M. & Oesterhelt, F. 2007 Monitoring dynamic systems with multiparameter fluorescence imaging. *Anal. Bioanal. Chem.* **387**, 71–82. (doi:10.1007/s00216-006-0917-0)

Kuhnemuth, R. & Seidel, C. A. M. 2001 Principles of single molecule multiparameter fluorescence spectroscopy. *Single Mol.* **2**, 251–254. (doi:10.1002/1438-5171(200112)2:4<251::AID-SIMO251>3.0.CO;2-T)

Ludden, M. L. W., Mulder, A., Schulze, K., Subramaniam, V., Tampe, R. & Huskens, J. 2008 Anchoring of histidine-tagged proteins to molecular printboards: self-assembly, thermodynamic modeling, and patterning. *Chem. Eur. J.* **14**, 2044–2051. (doi:10.1002/chem.200701478)

Maas, H., Khatyr, A. & Calzaferri, G. 2003 Phenoxazine dyes in zeolite L, synthesis and properties. *Microporous Mesoporous Mat.* **65**, 233–242. (doi:10.1016/j.micromeso.2003.08.014)

Maury, P., Escalante, M., Peter, M., Reinhoudt, D. N., Subramaniam, V. & Huskens, J. 2007 Creating nanopatterns of his-tagged proteins on surfaces by nanoimprint lithography using specific NiNTA–Histidine interactions. *Small* **3**, 1584–1592. (doi:10.1002/smll.200700046)

Megelski, S., Lieb, A., Pauchard, M., Drechsler, A., Glaus, S., Debus, C., Meixner, A. J. & Calzaferri, G. 2001 Orientation of fluorescent dyes in the nano channels of zeolite L. *J. Phys. Chem. B* **105**, 25–35. (doi:10.1021/jp002582c)

Miguez, H., Blanco, A., Meseguer, F., Lopez, C., Yates, H. M., Pemble, M. E., Fornes, V. & Mifsud, A. 1999 Bragg diffraction from indium phosphide infilled fcc silica colloidal crystals. *Phys. Rev. B* **59**, 1563–1566. (doi:10.1103/PhysRevB.59.1563)

Nair, D. K., Jose, M., Kuner, T., Zuschratter, W. & Hartig, R. 2006 FRET-FLIM at nanometer spectral resolution from living cells. *Opt. Express* **14**, 12 217–12 229. (doi:10.1364/OE.14.012217)

Nikles, D. & Tampe, R. 2007 Targeted degradation of ABC transporters in health and disease. *J. Bioenerg. Biomembr.* **39**, 489–497. (doi:10.1007/s10863-007-9120-z)

Nikolaev, I. S., Lodahl, P. & Vos, W. L. 2005 Quantitative analysis of directional spontaneous emission spectra from light sources in photonic crystals. *Phys. Rev. A* **71**, 053 813. (doi:10.1103/PhysRevA.71.053813)

Qu, J. L., Liu, L. X., Chen, D. N., Lin, Z. Y., Xu, G. X., Guo, B. P. & Niu, H. B. 2006 Temporally and spectrally resolved sampling imaging with a specially designed streak camera. *Opt. Lett.* **31**, 368–370. (doi:10.1364/OL.31.000368)

Ramamurthy, V., Sanderson, D. R. & Eaton, D. F. 1993 Control of dye assembly within zeolites—role of water and other coadsorbants. *J. Am. Chem. Soc.* **115**, 10 438–10 439. (doi:10.1021/ja00075a101)

Ruck, A., Hulshoff, C., Kinzler, I., Becker, W. & Steiner, R. 2007 SLIM: a new method for molecular imaging. *Microsc. Res. Tech.* **70**, 485–492. (doi:10.1002/jemt.20433)

Suhling, K., French, P. M. W. & Phillips, D. 2005 Time-resolved fluorescence microscopy. *Photochem. Photobiol. Sci.* **4**, 13–22. (doi:10.1039/b412924p)

Tinnefeld, P., Herten, D. P. & Sauer, M. 2001 Photophysical dynamics of single molecules studied by spectrally-resolved fluorescence lifetime imaging microscopy (SFLIM). *J. Phys. Chem. A* **105**, 7989–8003. (doi:10.1021/jp0103651)

Turchanin, A., Tinazli, A., El-Desawy, M., Grossann, H., Schnietz, M., Solak, H. H., Tampe, R. & Golzhauser, A. 2008 Molecular self-assembly, chemical lithography, and biochemical tweezers: a path for the fabrication of functional nanometer-scale protein arrays. *Adv. Mater.* **20**, 471. (doi:10.1002/adma.200702189)

Vietze, U., Krauss, O., Laeri, F., Ihlein, G., Schuth, F., Limburg, B. & Abraham, M. 1998 Zeolite-dye microlasers. *Phys. Rev. Lett.* **81**, 4628–4631. (doi:10.1103/PhysRevLett.81.4628)

Volkmer, A., Subramaniam, V., Birch, D. J. S. & Jovin, T. M. 2000 One- and two-photon excited fluorescence lifetimes and anisotropy decays of Green Fluorescent Proteins. *Biophys. J.* **78**, 1589–1598.

Ward, W. W. & Bokman, S. H. 1982 Reversible denaturation of aequorea green-fluorescent protein. *Biochemistry* **21**, 4535–4540. (doi:10.1021/bi00262a003)

Widengren, J., Kudryavtsev, V., Antonik, M., Berger, S., Gerken, M. & Seidel, C. A. M. 2006 Single-molecule detection and identification of multiple species by multiparameter fluorescence detection. *Anal. Chem.* **78**, 2039–2050. (doi:10.1021/ac0522759)

Wijnhoven, J. E. G. J., Bechger, L. & Vos, W. L. 2001 Fabrication and characterization of large macroporous photonic crystals in titania. *Chem. Mater.* **13**, 4486–4499. (doi:10.1021/cm0111581)

Yatskou, M. M., Meyer, M., Huber, S., Pfenniger, M. & Calzaferri, G. 2003 Electronic excitation energy migration in a photonic dye-zeolite antenna. *ChemPhysChem* **4**, 567–587. (doi:10.1002/cphc.200300567)

Zhang, K. C., Diehl, M. R. & Tirrell, D. A. 2005 Artificial polypeptide scaffold for protein immobilization. *J. Am. Chem. Soc.* **127**, 10 136–10 137. (doi:10.1021/ja051457h)

Zimmermann, T., Rietdorf, J. & Pepperkok, R. 2003 Spectral imaging and its applications in live cell microscopy. *FEBS Lett.* **546**, 87–92. (doi:10.1016/8s0014-5793(03)00521-0)